Plane dimpling and saddle-point bifurcation in the band structures of optimally doped high-temperature superconductors: A tight-binding model

O. K. Andersen, O. Jepsen, A. I. Liechtenstein, and I. I. Mazin
Max Planck Institut für Festkörperforschung, D-70569 Stuttgart, Federal Republic of Germany
(Received 30 July 1993; revised manuscript received 11 November 1993)

We argue that extended saddle points observed at the Fermi level for optimally doped superconductors are essentially the bifurcated saddle points predicted by density-functional [local density approximation (LDA)] calculations. Such saddle points are caused by the dimple of the CuO_2 planes and are enhanced by plane-plane hopping. Dimpling may provide a mechanism for pinning the Fermi level to the saddle points. Simple tight-binding Hamiltonians and analytical expressions for the constant-energy contours are derived from the LDA bands of $YBa_2Cu_3O_7$. In addition to the usual O2 x, O3 y, and Cu x^2- y^2 orbitals, we find that O2 z and O3 z are crucial and Cu s, xz, and yz important. The O z orbitals allow the $pd\sigma$ antibond to tilt with the dimple.

I. INTRODUCTION

One of the surprises in high-temperature superconductivity research is that it has been possible to map out band structures of several high-temperature superconductors (HTSC's) using angle-resolved photoemission,[1–4] that the Fermi surfaces (FS's) agree in detail with the predictions of density-functional [local density approximation (LDA)] theory,[5,6] and that the velocity-renormalizations are less than about 3.

In particular, the Fermi levels of *double-plane* materials like $YBa_2Cu_3O_7$ and $YBa_2Cu_4O_8$ with near *optimal doping* seem to be *within 30 meV of anomalous saddle points* positioned near $(k_xa/\pi, k_yb/\pi)$=(1,0) and (0,1). With the appropriate transformation of axes, this holds for $Bi_2Sr_2CaCu_2O_{8+\delta}$, too. As regards the nature of the saddle-point anomaly, the LDA prediction[6] was that the saddle points are *bifurcated*, away from the high-symmetry positions, to the positions $(1\pm\Delta k,0)\pi/a$ and $(0,1\pm\Delta k)\pi/b$ with $\Delta k \approx 0.3$. The constant-energy contour through the saddle points therefore behaves like the circles in Fig. 1, rather than in the conventional way indicated by the straight (dashed) lines. Angle-resolved photoemission[4] now yields that the band has an anomalously *flat* (k^4-like), downwards dispersion towards (0,0) and a normal (k^2-like), upwards dispersion towards (1,1); in other words, that $\Delta k \to 0$ so that the circles in the schematic Fig. 1 *touch* at the high-symmetry points (1,0) and (0,1). This kind of saddle point is called *extended*.[4] The slight discrepancy in the degree of bifurcation between the predicted, $\Delta k \approx 0.3$, and the measured, $\Delta k \to 0$, is hardly surprising considering the facts that the LDA neglects electronic correlations and photoemission probes only the surface region.

The band with the saddle points near ϵ_F is that antibonding $pd\sigma$-like plane band whose wave functions are *odd* (o) with respect to the mirror plane between the two neighboring CuO_2 planes. For $YBa_2Cu_3O_7$, angle-resolved photoemission[7] also confirms the LDA prediction (Fig. 2) for the *even* (e) antibonding $pd\sigma$-like plane band, positron annihilation[8] confirms the prediction for the FS sheet from the antibonding $pd\sigma$-like chain band (c), and de Haas–van Alphen experiments[9] seem to confirm the LDA prediction[10,11] for the so-called stick sheet (s) of the FS which arises from the uppermost $pd\pi$-like chain band. Figure 2 exhibits the cross sections of the LDA FS and the neighboring constant energy surfaces

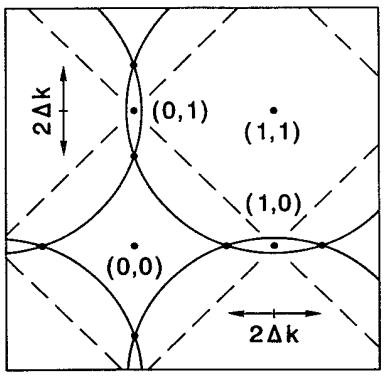

FIG. 1. FS of an optimally doped high-temperature superconductor (schematic). The FS passes through saddle points which are *bifurcated* by $2\Delta k$. For $\Delta k \to 0$, the circles (cylinders) would *touch* at the high-symmetry points (1,0) and (0,1), in which case the saddle points would have k^4 dispersion in the [10] or [01] directions (but the usual k^2 dispersion in the perpendicular direction), i.e., they would be *extended*. For $YBa_2Cu_3O_{6.92}$, the corresponding FS sheet would be the one for the *odd* plane band. In the LDA for $YBa_2Cu_3O_7$, this band has considerable k_z dispersion due to interaction with the chain bands. The interaction with the dominant chain $pd\sigma$ band, however, vanishes by symmetry when k_z=0, and the corresponding LDA contour for the saddle-point energy resembles the intersecting circles [see (o,0)-contours in the left part of Fig. 2], in particular if also the interaction with the chain $pd\pi$ band could be neglected. The dashed lines show a FS passing through the saddle points of a band with normal $k_x^2 - k_y^2$ dispersion.

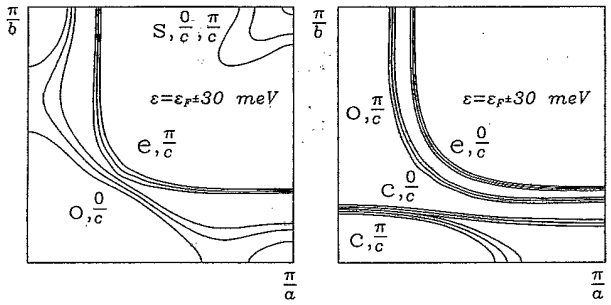

FIG. 2. LDA FS and constant energy surfaces corresponding to $\epsilon = \epsilon_F \pm 30$ meV for $YBa_2Cu_3O_7$, calculated with the FP LMTO method. The FS has four sheets, the plane $pd\sigma$-like odd (o) and even (e) sheets, and the chain $pd\sigma$ (c) and $pd\pi$ (s) sheets. Shown are the cross sections with the k_z=0 and π/c planes. The cross sections in the left part of the figure are those which do not hybridize with the (c) band.

(±30 meV) with the $k_z = 0$ and π/c planes. We shall return to this figure several times (and shall also explain the reason for splitting the contours into a left and right figure).

Many, if not all, anomalous properties of the HTSC's near optimal doping are consistent with a scenario[12,13] with the Fermi level close to a (normal) saddle point in a two-dimensional (2D) band structure ($\epsilon \propto k_x^2 - k_y^2$). At optimal doping, ϵ_F is at the saddle point and this yields a logarithmic van-Hove singularity in the density of states and a singularity in $\mathrm{Im}\chi(\mathbf{q},\omega)$, for ω small and $\mathbf{q}$ sliding along the flat part of the FS.[12–14] If present, such phase-space effects would also be favorable for an electronic pairing mechanism and, together, these two features could explain the small isotope effect at optimal doping.[15] Now, the existence of *extended* saddle points (i.e., k^4 rather than k^2 dispersion in one of the directions), would enhance the phase space effects,[16] or even make an excitonic mechanism for HTSC a realistic possibility. At the least, it could partly compensate for a finite dispersion in the third space direction, if present. The LDA predicts considerable k_z dispersion for $YBa_2Cu_3O_7$, in particular near the saddle points, where it is caused by coupling through the chain bands. This may be seen from Fig. 2. The three-dimensional, bifurcated LDA bands do *not* give rise to a spectacular singularity in the density of states,[6] but decreasing the bifurcation to zero as hinted by the photoemission experiment would sharpen up the 3D van Hove singularities.

In addition to a 30 meV gap in the spin-fluctuation spectrum, neutron scattering on $YBa_2Cu_3O_{7-x}$ exhibits a strong peak at $(q_x a/\pi, q_y b/\pi)$=(1,1) and ω=41 meV,[17] whose width Δq increases with the hole doping n_h.[18] This is consistent with the NMR data, but *not* with the LDA prediction of $\chi''(\mathbf{q},\omega)$,[6,19] which has no commensurate (1,1) peak because ϵ_F is ~20 meV above both saddle points, and because the minima at the high-symmetry points are not sufficiently shallow. A small adjustment of this band and its Fermi level would, however, bring them into agreement with the situation sketched in Fig. 1, where the flat band in the (1,0) segment "nests" onto the one in the (0,1) segment. This adjustment also makes the band structure consistent with the observed uniaxial pressure dependence of T_c,[20] which indicates that the (1,0) saddle is slightly above, and the (0,1) saddle slightly below ϵ_F. A curious observation is that whereas heavy doping has made the spin-fluctuation coherence length short inside the planes, the coupling between two planes remains strong and antiferromagnetic.[18] We shall return to this point at the end of the paper.

The LDA bands in Ref. 6 prove that the degree of calculated bifurcation (Δk) is controlled by the *dimple* of a CuO_2 plane, which is a displacement in the perpendicular direction of the oxygens with respect to the copper. In $YBa_2Cu_3O_7$, this oxygen displacement in the c direction is *towards* the neighboring CuO_2 plane, and it amounts to $0.064a \approx 0.25$ Å for the O2 rows (in the a direction) and to $0.070a$ for the O3 rows. Figure 3 displays two LDA electronic band structures[6] calculated with respectively increased (full line) and decreased (dashed line) dimplings by $\pm 0.03a$. The bands are for $k_z = 0$ and $(k_x a/\pi, k_y b/\pi)$ along the high symmetry lines from Γ (0,0) to X (1,0), to S (1,1) to Y (0,1), back to Γ and, finally, along the [1,1] diagonal to S. The bifurcated saddle points are seen as one maximum along ΓX and one along ΓY. In Ref. 6 also the adiabatic bands for the corresponding copper mode are shown, and they are nearly identical to those in Fig. 3, except for an exchange of the full and dashed lines. Clearly, with decreasing dimple, the bifurcation Δk decreases and the saddle point becomes extended ($\Delta k \to 0$) for a critical value of the dimple which, as judged from the figure, lies between $0.040a$ and $0.034a$ in $YBa_2Cu_3O_7$. For even smaller values of the dimpling, in particular for a completely *flat* plane, the saddle points are at X and Y, and the dispersion is *quadratic* ($\propto k^2$ in all directions). The *ab initio* LDA frozen-phonon calculations of which Fig. 3 is a by-product, reproduce within 10% the size of the dimpling in $YBa_2Cu_3O_7$, as well as the frequencies of the dimpling modes,[6,21–23] which have been studied extensively with Raman scattering (Cu2: 150 cm^{-1}, O3–O2: 330 cm^{-1}, and O3+O2: 440 cm^{-1}).[24,25] Even the calculated coupling of these modes to electrons in the superconducting state ($\lambda \approx 1$) agree well with Raman-scattering results.[26]

If the Fermi level is really within 30 meV, i.e., phonon energies, of the saddle points, the high T_c might be ex-

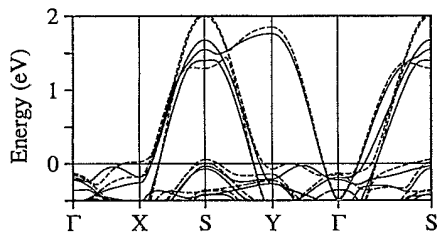

FIG. 3. Adiabatic LDA energy bands for the in-phase dimpling mode (440 cm^{-1}) in $YBa_2Cu_3O_7$. The full (dashed) bands are for increased (decreased) dimpling with oxygen displacements of $0.03a$. The self-consistent calculations were performed with the FP LMTO method and 147 points in the irreducible zone. The Fermi level is the zero of energy.

plained by the electron-phonon mechanism with $\lambda \sim 1$ because this violation of Migdal's theorem invalidates the usual Eliashberg theory. Recent studies[27] indicate that such nonadiabatic effects tend to increase T_c and to yield an anomalous behavior of the isotope effect, as observed.

It could seem as if, for doping levels within a certain range, the dimpling would adjust itself so as to *pin* the bifurcated saddle points to the Fermi level: This range of *optimal* doping would then set in when the saddle points at ϵ_F become extended, and would continue through some range of bifurcations. Since the FS sheets passing through the saddle points are, to a first approximation, intersecting circles (Fig. 1), the relation between the optimal number of holes $\bar{n}_h$ (in excess of 1) and the bifurcation Δk is approximately

$$\bar{n}_h(\Delta k) \sim \frac{\pi}{2}\left[1+(\Delta k)^2\right] - 1 - 2(\Delta k)^3 \qquad (1)$$

with Δk in units of π/a, and where the last term is the number of holes in the segments between the bifurcated saddle points. The onset of optimal doping would thus be at $\bar{n}_h(0) \sim \frac{\pi}{2}\text{-}1 \sim 0.6$ holes per double plane in the odd FS sheet. Since the LDA calculations show that the even sheet is approximately half full (see Fig. 2), essentially *all the doped holes go into the odd sheet*, and this means that the total number of holes at the onset of optimal doping is $\sim$0.6, *provided* that there is no k_z dispersion. The LDA, however, gives considerable dispersion for $YBa_2Cu_3O_7$, in particular near the saddle points, as seen in Fig. 2, so that the area inside the $k_z = \pi/c$ contour of the odd plane sheet is only about half the 2D Brillouin zone. This means that for the 3D LDA bands, the right-hand side of Eq. (1) should be divided by $\sim$2. With 3D bands, the onset of optimal doping thus takes the more conventional value: $\bar{n}_h(0) \sim 0.28$ holes per double plane, and the doping corresponding to the LDA bifurcation for $YBa_2Cu_3O_7$ is $\bar{n}_h(0.3) \sim 0.33$ per double plane.

It thus seems important to study *in detail* the implications for superconductivity of extended or slightly bifurcated saddle points close to the Fermi level. With the many ideas around, there is a lot to be done. In the present paper we shall therefore hunt the electronic degrees of freedom which enable the bifurcation: Based on analysis of the LDA bands for $YBa_2Cu_3O_7$, we derive a simple *tight-binding model with an analytical expression for the FS*. This model gives an LDA *realistic* description of the bifurcation for double, as well as for single CuO_2 layers, and we find that the most important electronic degrees of freedom, in addition to the usual O2 x, O3 y, and Cu x^2-y^2 orbitals, are the plane-oxygen z orbitals which allow the $pd\sigma$ antibond to *tilt* with the dimple. Our model contains the hopping interaction between the two planes but we deliberately avoid the hopping through the chain, which is specific for $YBa_2Cu_3O_{7-x}$ materials and which might be prohibited by scattering, anyhow. The model is therefore basically 2D but, if wanted, it is an easy task to reinstall k_z dispersion in the odd and even planelike bands by fitting also to the contours in the right part of Fig. 2. It is our hope that the model will be used in the future for the single-particle terms in more sophisticated Hamiltonians containing, for instance, the Coulomb correlations, the phonons, and the electron-phonon interaction. Presently we are working on providing the parameters for the latter. Towards the end of the paper (Sec. V), we give a tutorial on the development of the constant energy surfaces as functions of the band filling and the various physical parameters. In Sec. VI, we give the simplest possible translationally invariant mathematical model for the constant energy surfaces near the Fermi energy of a dimpled plane.

II. ANALYSIS OF THE LDA BANDS

A. LDA Fermi surface for $YBa_2Cu_3O_7$

In Fig. 2 we show cross sections of the LDA Fermi surface and adjacent ($\pm$30 meV) constant-energy surfaces for $YBa_2Cu_3O_7$ with the k_z=0 and π/c symmetry planes.[6,22,11] As specified in Refs. 21, 6, 11, and 23, these constant-energy contours (CEC's) were calculated with the highly accurate full-potential linear muffin tin orbital (FP LMTO) method using $\sim$800 first-principles points in the irreducible part of the Brillouin zone and 147 points in the self-consistency cycle. We now first describe this LDA FS and then fold down remote orbitals (e.g., Y, Ba, Cu *sp*, O *s*), remove the Cu *d* and O *p* chain orbitals, and analyze the pure plane sheets quantitatively.

The left panel shows those CEC's which do *not* hybridize with the dominant *chain* $pd\sigma$ band (c); they belong to the odd (o) plane sheet for k_z=0, to the even (e) plane sheet for k_z=π/c, and to the uppermost chain $pd\pi$ band (the stick, s) for k_z=0 and π/c. As mentioned in the Introduction, for the *plane* bands, odd and even refer to the character of the wave functions with respect to the mirror plane perpendicular to the c axis and between the planes, through the yttrium atoms. The wave functions of the *chain* $pd\sigma$ and $pd\pi$ bands are respectively even and odd with respect to the mirror plane perpendicular to the c axis and containing the chains. Now, the stick band lies well below the plane bands except along the ΓS [1,1] line (see Fig. 3) where it pushes them up slightly and gives rise to the "wiggles" seen in the (o,0) and (e,π/c) contours in the left panel of Fig. 2. Apart from this, *the plane states (o,0) and (e,π/c) do not hybridize with chain states.* The (o,0) CEC's clearly exhibit saddle points less than 20 meV below ϵ_F at the points $(\bar{k}_x, 0)$ and $(0, \bar{k}_y)$. Since the $(\pi/a, k_y, k_z)$ and $(k_x, \pi/b, k_z)$ - planes are mirrors, these saddle points are bifurcated away from the symmetry positions $(\pi/a, 0)$ and $(0, \pi/b)$. As mentioned above, the area inside the (e,π/c) CEC is slightly less than half the area of the 2D Brillouin zone and it is as if the (o,0) CEC has taken up slightly more than all the holes provided by the chain. The e sheet also has bifurcated saddle points for k_z=π/c, but they are 0.8 eV below the Fermi level.

In the right panel of the figure we show the chain $pd\sigma$ sheet (c) and those plane CEC's (o,π/c) and (e,0) which interact with it. Near ϵ_F, the *ec* mixing is weak and the *oc* mixing strong. In both cases, however, the saddle points are outside the $\pm$30 meV range. The e sheet,

in fact, has bifurcated saddle points for k_z=0 at 0.7 eV below ϵ_F, and the *o* sheet has bifurcated saddle points for $k_z=\pi/c$ at 0.4 eV below the Fermi level. The *c* sheet has a nonbifurcated saddle point at $\mathbf{k}=(\pi/a,0,\pi/c)$ merely 80 meV above ϵ_F with considerable *o* character.

Due to this rather strong k_z dispersion of the LDA bands, the van Hove singularities near the Fermi level are three-dimensional and *not* prominent. In this paper, we are not interested in the specifically chain-related features and we shall therefore not consider the k_z dispersion further. What are of interest are the odd and even plane-band contours in the left panel, released from the influence of the chain derived stick band.

B. Breaking down of the band structure

In order to analyze these bands quantitatively, we are forced to use the LMTO method in the atomic-spheres approximation (ASA) because this is presently the only scheme which employs a first-principles tight-binding representation and which provides an *accurate* way of *downfolding* orbitals.[28] However, with carefully chosen sphere sizes, the ASA bands are quite close to those calculated with the full-potential version, as for instance a comparison of the CEC's in the left panels of Figs. 2 and 7 demonstrates (these two figures should, in fact not be quite identical, because the influence of the stick band has been deliberately removed from the bands in Fig. 7). The downfolding now starts with an *exact transformation* to a representation in which the *tails* of the orbitals, which are to remain in the basis, e.g., O2 *x*, are radial Schrödinger-equation solutions at *one* energy, chosen at the center of interest (here ϵ_F), for the channels to be downfolded, e.g., Y *d*. After this transformation, the orbitals corresponding to the downfolded channels are *removed* from the basis. The remaining orbitals are energy independent, but not necessarily orthogonal or short ranged.

In Fig. 4(a) we show the LMTO-ASA band structure for k_z=0 along the triangle $(k_xa/\pi, k_yb/\pi)$ = (0,0)-(1,0)-(1,1)-(0,0) in a 4 eV range around the Fermi level. The band structure is nearly identical with the average between the two full-potential band structures shown in Fig. 3 [note that the third panel in Fig. 4(a) shows the $S\Gamma$ and not the SY direction as in Fig. 3]. The band structure consists of the antibonding $pd\sigma$ chain (*c*) band, and the $pd\sigma$ even (*e*) and odd (*o*) plane bands rising above the top of the Cu *d* - O *p* complex. The *o* band of course lies above the *e* band. As mentioned above, the *o* band does not hybridize with the *c* band, and its (1,0) saddle point is clearly bifurcated to (1±0.3,0). Figure 4(b) shows the bands along the same triangle in the $k_z=\pi/c$ plane where now *o* and *c*, but *not e* and *c*, mix. This hybridization with the chain band pushes the saddle point of the *o* band to (1,0,1), i.e., it removes the bifurcation in this zone-boundary plane. The calculations in Figs. 4(a) and 4(b) were performed with the Cu *sp*-, the O *s*- and *d*-, the Ba and Y *spdf*-, and all interstitial-sphere channels folded down. The basis thus included *only* the Cu *d* and the O *p* orbitals. In the energy range shown, *this had no visible effects.*

In the following Figs. 4(c)–4(j), we removed (without down folding) all remaining orbitals except plane Cu x^2-y^2, *zx*, and *zy*, plane O2 *x* and *z*, and plane O3 *y* and *z*. These 2×7 orbitals are centered *exclusively on the two planes* so that the k_z dispersion is removed and the

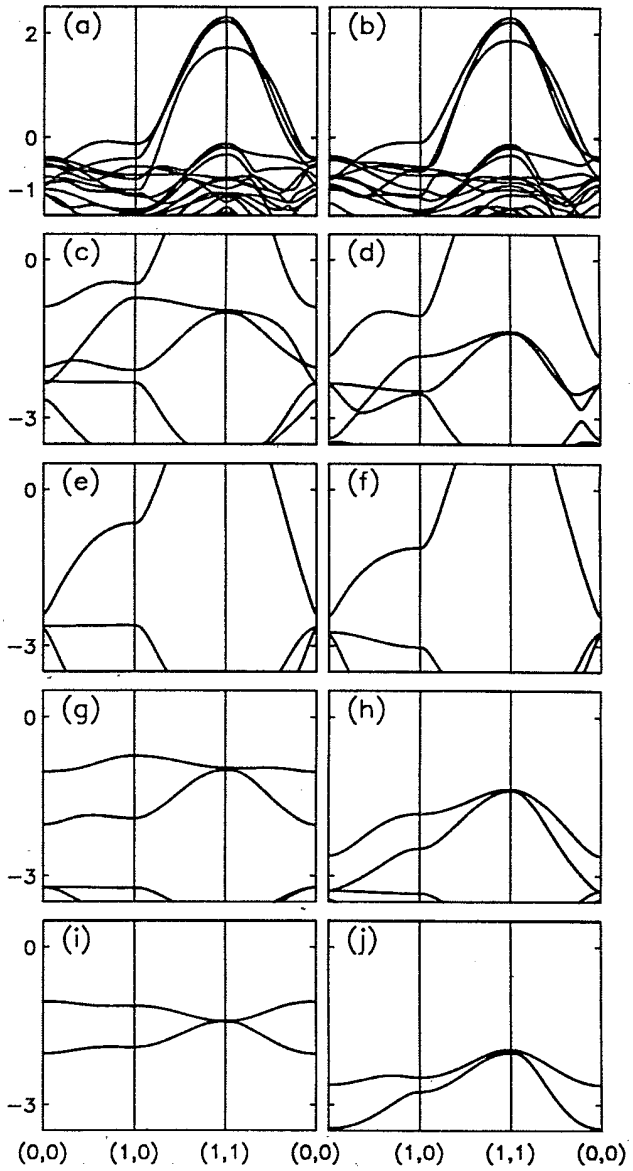

FIG. 4. Breaking up of the $YBa_2Cu_3O_7$ band structure. These LDA calculations were performed with the LMTO ASA method and various basis sets. (a) (k_z=0) and (b) ($k_z=\pi/c$): Accurate downfolded (O *p*, Cu *d*) basis. Left panels (c), (e), (g), and (i): Odd (*o*) linear combinations. Right panels (d), (f), (h), and (j): Even (*e*) linear combinations. (c) and (d): Hybridized $pd\sigma$ and $pd\pi$ bands, i.e., the basis included the O2 *x*, *z*, O3 *y*, *z*, Cu x^2-y^2, *zx*, and *zy* LMTO's. (e) and (f): Pure $pd\sigma$ bands, i.e., the basis included the O2 *x*, O3 *y*, and Cu x^2-y^2 LMTO's. (g) and (h): Pure $pd\pi$ bands, i.e., the basis included the O2 *z*, O3 *z*, and Cu *zx*, *zy* LMTO's. (i) and (j): Pure oxygen *z* bands, i.e., the basis included the O2 *z* and O3 *z* orbitals.

states are strictly odd or even with respect to the mirror plane through yttrium. The bands calculated (using the original LDA ASA potential) with *odd* linear combinations of these orbitals are shown in the figures to the left (c, e, g, and i) and those calculated with *even* linear combination are shown in the figures to the right (d, f, h, and j).

Figures 4(c) and 4(d) result from calculations with all 7 odd or all 7 even orbitals in the basis. Apart from a 0.4 eV energy shift, the (uppermost) *o* band in Fig. 4(c) is *very nearly identical* to that resulting from the more complete calculation in Fig. 4(a) and, hence, to that of the FP-LMTO calculation in Fig. 3. The same holds for the (uppermost) *e* band in Fig. 4(d) compared with Fig. 4(b) where, at (1,0), the *e* band is the fourth from the top. In particular, the saddle points of both bands are bifurcated, but to different extents. We would like to point out, that inclusion of the Cu $3z^2$-1 and apical O *z* orbitals *hardly* influenced the dispersion of the *o* and *e* bands and, as a consequence, we left them out. It is at the level of Figs. 4(c) and 4(d), that we want to reproduce the LDA bands with a simple but physical tight-binding model.

We now remove further orbitals. In Figs. 4(e) and 4(f), the Cu *zx*, and *zy*, and the O *z* orbitals were removed. The remaining basis is thus the $pd\sigma$ orbitals of the usual 3-band model, albeit for two planes and using carefully constructed *ab initio* orbitals. The characters of these three bands are thus antibonding CuO, nonbonding O, and bonding CuO. The latter band is mostly below the frame of the figure. The interplane coupling, measured as the shift between the *o* and *e* bands, is about 0.5 eV at (1,0) and nearly vanishes along the (0,0)–(1,1) line. *This interplane hopping is due to the Cu s character* which has been folded into the tails of the O2 *x* and O3 *y* orbitals. A calculation without folding the Cu *s* orbitals down, but keeping them explicitly in the basis, revealed that their energies are 4.8 eV (*o*) and 3.5 eV (*e*) at the Γ point. That the Cu *s* character dominates over the $3z^2$-1 character, which has the same symmetry in the plane but pushes the saddle points up rather than down in energy, can be seen from the $|\psi|^2$ plots in Fig. 3 of Ref. 6 and in Figs. 3(b) and 4 of Ref. 11. A schematic picture of the Cu *s* hybridized $pd\sigma$ orbitals at (1,0) and (0,1) are given in the upper part of Fig. 5.

Figures 4(g) and 4(h) display the $pd\pi$ bands obtained exclusively with those orbitals removed from the 7 set to obtain the 3-band results of Figs. 4(e) and 4(f); these orbitals are O2 *z*, O3 *z*, Cu *zx*, and *zy*. Comparison of the superpositions of Figs. 4(g) and 4(e), and of Figs. 4(h) and 4(f), with respectively Figs. 4(c) and 4(d), *unveils the bifurcation mechanism as hybridization between the antibonding plane* $pd\pi$ *and* $pd\sigma$ *orbitals. The coupling is from plane-oxygen z to Cu* x^2-y^2 *and it vanishes without the dimple.* In Figs. 4(g) and 4(h) we recognize the even and odd $pd\pi$ bands split by roughly an eV and notice that their dispersions are quite different. The reason is that much of the *interplane coupling is mediated by yttrium* so that the even and odd states couple through *different* channels, e.g., Y *sd* and *pf*. The uppermost *o* and *e* bands along (0,0)–(1,0) arise from the antibonding (O2 *z*, Cu *zx*) orbitals and *the dispersions of these bands determine the details of the bifurcation. Right at* (1,0) *they cannot couple to the* $pd\sigma$ *orbitals* because, as shown in Fig. 5, these have a node through O2. At (1,0) the coupling is only to the O3 *z* orbitals which are involved in the second *o* and *e* (O3 *z*, Cu *zy*) $pd\pi$ bands. This is the origin of the minimum at (1,0).

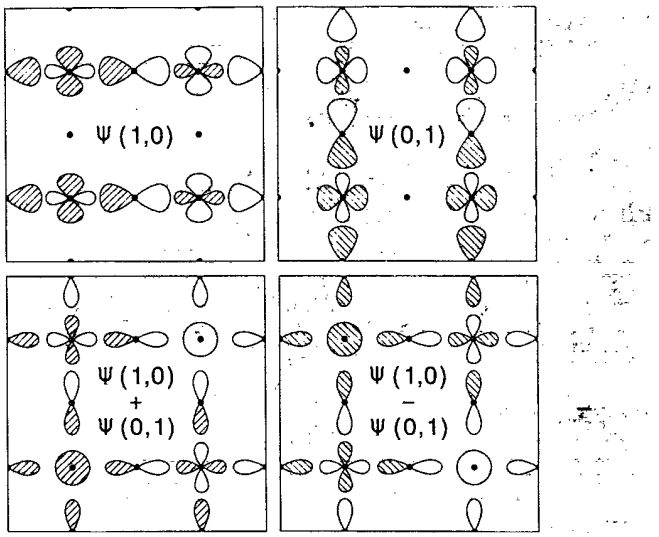

FIG. 5. Schematic plane-band wave functions at the high-symmetry points (1,0) and (0,1), as well as their sum and difference, which are the relevant linear combinations for an antiferromagnetic spin fluctuation.

In Figs. 4(i) and 4(j), we finally omitted the Cu *zx* and *zy* orbitals and retained only the O *z* orbitals. Since the splitting between the *o* and *e* bands is as large between Figs. 4(i) and 4(j) as between Figs. 4(g) and 4(h), we realize that the O *z* orbitals rather than the Cu *zx* and *zy* orbitals, provide most of the interplane coupling (see also Figs. 5 and 6 in Ref. 11). Even more than for the Cu *s*-Cu *s* interplane hopping, the O *z* - O *z* hopping proceeds partly via Y. The same is true for the O2 *z* - O3 *z* intraplane hopping which gives rise to the large splittings at the Γ point. At Γ, there is no coupling to the Cu *zx* and *zy* orbitals but at (1,0) there is, as seen by comparison between Figs. 4(i) and (g), and between Figs. 4(j) and 4(h). It is possible to obtain bifurcation by adding merely the O2 and O3 *z* orbitals to the three band model, thus leaving out the Cu *zx* and *zy* orbitals, but the band then tends to be too flat between (0,0) and (1,0).

We now write down the simplest possible tight-binding model which reproduces Figs. 4(c) and 4(d) (using two different sets of parameters). Since we shall force our tight-binding model to be orthonormal (the overlap matrix is the unit matrix) and to have near-neighbor interactions only, agreement with Figs. 4(c) and 4(d) can only be achieved over a limited energy range. This we choose to be centered at the saddle points. It turns out that in order to get an acceptable description with near-neighbor hoppings only, we need to include the Cu *s* orbital explicitly. We therefore start out with a physical 8-band

model and then later fold down the Cu s, xz, and yz orbitals into the tails of the neighboring oxygen orbitals, at the expense of having to include second neighbor O-O hoppings in the resulting 5-band Hamiltonian.

III. EIGHT AND FIVE-BAND HAMILTONIANS

Since the wave functions split in even and odd, we formally need only consider a single plane with different parameter values for the even and odd states. The copper positions are $\mathbf{R} \equiv (na, mb, 0)$, and the oxygen positions are $\mathbf{R}_{O2} \equiv \mathbf{R} + (1, 0, \tan\delta_a)\, a/2$ and $\mathbf{R}_{O3} \equiv \mathbf{R} + (0, 1, \tan\delta_b)\, b/2$. Here, n and m take all integer values and δ is the dimpling angle, which we allow to be different in the a and b directions. As basis states we first take the following eight Bloch orbitals:

$$
\begin{aligned}
|d\rangle &\equiv \textstyle\sum_{nm} |\text{Cu } x^2-y^2\rangle \exp(i\mathbf{k}\cdot\mathbf{R}),\\
|s\rangle &\equiv \textstyle\sum_{nm} |\text{Cu } s\rangle \exp(i\mathbf{k}\cdot\mathbf{R}),\\
|x\rangle &\equiv \textstyle\sum_{nm} |\text{O2 } x\rangle\, i^{-1} \exp(i\mathbf{k}\cdot\mathbf{R}_{O2}),\\
|y\rangle &\equiv \textstyle\sum_{nm} |\text{O3 } y\rangle\, i^{-1} \exp(i\mathbf{k}\cdot\mathbf{R}_{O3}),\\
|za\rangle &\equiv \textstyle\sum_{nm} |\text{O2 } z\rangle \exp(i\mathbf{k}\cdot\mathbf{R}_{O2}),\\
|zb\rangle &\equiv \textstyle\sum_{nm} |\text{O3 } z\rangle \exp(i\mathbf{k}\cdot\mathbf{R}_{O3}),\\
|zx\rangle &\equiv \textstyle\sum_{nm} |\text{Cu } zx\rangle\, i^{-1} \exp(i\mathbf{k}\cdot\mathbf{R}),\\
|zy\rangle &\equiv \textstyle\sum_{nm} |\text{Cu } zy\rangle\, i^{-1} \exp(i\mathbf{k}\cdot\mathbf{R}),
\end{aligned}
$$

which we assume are orthonormal. The corresponding 8-band Hamiltonian H^8 is then

H^8	$\lvert d\rangle$	$\lvert s\rangle$	$\lvert x\rangle$	$\lvert y\rangle$	$\lvert za\rangle$	$\lvert zb\rangle$	$\lvert zx\rangle$	$\lvert zy\rangle$
$\langle d\rvert$	ϵ_d	0	$t_{xd}s_x$	$-t_{yd}s_y$	$t_a c_x$	$-t_b c_y$	0	0
$\langle s\rvert$	0	ϵ_s	$t_{sx}s_x$	$t_{sy}s_y$	0	0	0	0
$\langle x\rvert$	$t_{xd}s_x$	$t_{sx}s_x$	ϵ_x	0	0	0	0	0
$\langle y\rvert$	$-t_{yd}s_y$	$t_{sy}s_y$	0	ϵ_y	0	0	0	0
$\langle za\rvert$	$t_a c_x$	0	0	0	ϵ_{za}	$-t_{zz}c_x c_y$	$t_{z,xx}s_x$	0
$\langle zb\rvert$	$-t_b c_y$	0	0	0	$-t_{zz}c_x c_y$	ϵ_{zb}	0	$t_{z,zy}s_y$
$\langle zx\rvert$	0	0	0	0	$t_{z,xx}s_x$	0	ϵ_{zx}	0
$\langle zy\rvert$	0	0	0	0	0	$t_{z,zy}s_y$	0	ϵ_{zy}

(2)

where $s_x \equiv 2\sin(ak_x/2)$, $c_y \equiv 2\cos(bk_y/2)$, and so on. We have only included hopping between nearest-neighbor atoms, except for the hopping t_{zz} from O2 z to O3 z. This is the hoppping which yields the splitting of the $pd\pi$ bands at Γ [Figs. 4(g)–4(j)] and which proceeds via nearest-neighbor hopping to yttrium (and to barium).

The values of the parameters were obtained by fitting to the odd and even LDA LMTO-ASA bands in Figs. 4(c) and 4(d). The *starting values* were obtained by fitting individual parameters at the high-symmetry points to the pure $pd\sigma$ (hybridizing with Cu s) and $pd\pi$ odd bands in Figs. 4(e) and 4(g), and to the even bands in Figs. 4(f) and 4(h): Setting t_a=t_b=0 in H^8, we immediately see that the eigenvalues at the Γ point are ϵ_s, ϵ_d, ϵ_x, ϵ_y, ϵ_{zx}, ϵ_{zy}, and

$$
\frac{\epsilon_{za}+\epsilon_{zb}}{2} \pm \sqrt{\left(\frac{\epsilon_{za}-\epsilon_{zb}}{2}\right)^2 + (4t_{zz})^2} \approx \epsilon_z \pm 4t_{zz},
$$

neglecting the orthorhombicity of the O z orbital energy. The Γ-point energies thus immediately provide the orbital energies and the O z - O z hopping integral. It takes a bit of care to decide which energy is ϵ_x and which is ϵ_y. To a first approximation ϵ_x=ϵ_y, so that this is the energy of the nearly degenerate $pd\sigma$ band. By considering the small-k behavior, one may then realize that ϵ_y is the k=0 limit of the band which is flat when going to (0,0) along the [1,0] direction, and vice versa for ϵ_x. The initial values for the remaining hopping integrals may now be determined from the energies at $(k_x\pi/a, k_y\pi/b)$ =(1,0), (0,1), and (1,1): At (1,1) the hybridization between $pd\sigma$ and Cu s vanishes, provided that we neglect the orthorhombicities, and we see that $8t_{pd}^2 = (\epsilon-\epsilon_d)(\epsilon-\epsilon_p)$, where ϵ is the top of the $pd\sigma$ band at (1,1) and the subscript p is x and y. The value of the O x - Cu s hopping integral t_{sx} is now obtained from the saddle-point energy ϵ at (1,0) using the equation

$$
\frac{4t_{xd}^2}{(\epsilon-\epsilon_x)(\epsilon-\epsilon_d)} - \frac{4t_{sx}^2}{(\epsilon_s-\epsilon)(\epsilon-\epsilon_x)} = 1, \tag{3}
$$

which we shall derive in Sec. IV. Similarly, t_{sy} may be found from the energy at (0,1), although for the initial values we take it equal to t_{sx}. The O2 z - Cu zx hopping integral is found from the energy ϵ at (1,0) of the uppermost $pd\pi$ band [Figs. 4(g) or 4(h)] using $4t_{z,xx}^2 = (\epsilon-\epsilon_z)(\epsilon-\epsilon_{zx})$, and $t_{z,zy}$ is taken equal to $t_{z,zx}$.

Starting from these initial values, the parameters were then refined in a least squares fit with an energy dependent weighting given by the derivative of a Fermi function centered at the (1,0) saddle-point energy and of half width kT=0.2 eV. The resulting *final* values for the orbital energies were the following:

meV	ϵ_d	ϵ_s	ϵ_x	ϵ_y	ϵ_{za}=ϵ_{zb}	ϵ_{zx}=ϵ_{zy}
o	−2308	+4844	−3199	−3082	−1602	−3639
e	−2402	+3378	−3476	−3267	−2304	−3056

where forcing $\epsilon_{xa} = \epsilon_{xb}$ and $\epsilon_{zx} = \epsilon_{xy}$ did not deteriorate the fit. The zero of energy is here the original Fermi energy of the "all-orbital" calculation [Figs. 4(a) and 4(b)] which yielded somewhat higher energies than the 7-LMTO band structure to which we are fitting. We now define the Fermi energy as the one which gives constant energy contours for the 7-LMTO calculation most similar to the $(o,0)$ and $(e,\pi/c)$ contours in the left part of Fig. 2. This yields $\epsilon_F = -417.5$ meV.

The half difference between two orbital energies $(\epsilon_i^o - \epsilon_i^e)/2 \equiv t_i^c$ is the effective interplanar (or perpendicular) hopping integral for orbital $|i\rangle$. As expected, it is particularly large (~733 meV) for Cu s - Cu s hopping, and sizable for O z - O z hopping (~351 meV). For the effective Cu zx - Cu zx and zy interplanar hopping integrals we find a surprisingly large, *negative* value (-292 meV) which we ascribe to the hopping through yttrium.

The *final* values for the in-plane hopping integrals were:

meV	t_{xd}	t_{yd}	t_{sx}	t_{sy}	t_{zz}	$t_{z,zx}$	$t_{z,xy}$	t_a	t_b
o	1576	1556	2024	2006	120	829	831	228	223
e	1599	1588	2582	2517	12	543	524	267	249

and the reason why the hopping integrals in the a direction are usually a bit larger than in the b direction is that $b/a \approx 1.017$. In fact, the orthorhombicity of the hopping integrals is considerably smaller than expected from the canonical scaling law: $t_{ll'} \propto (a/b)^{l+l'+1}$ which yields 1.03 and 1.07 for sp and pd hopping, respectively.

The hoppings t_a and t_b from an oxygen z to the Cu x^2-y^2 orbital *vanish for a flat plane* and we expect them to behave like

$$t_a \propto a^{-4} \sin \delta_a \quad \text{and} \quad t_b \propto b^{-4} \sin \delta_b, \tag{4}$$

as a function of the appropriate dimpling angle and lattice constant. Since $\delta_b/\delta_a \approx 1.08$, this expression predicts a near cancellation of the orthorhombicity effects from the lattice constants and from the dimpling angles. The fitted parameter values indicate that the former effect dominates. In principle, there are similar hopping integrals from the oxygen x and y orbitals to the Cu zx and zy orbitals, but we assume that they can be absorbed in t_a and t_b.

The fact that the hopping integrals for the odd and even orbitals are not identical is due to nonperpendicular interplane hopping, e.g., from O2 z in one plane to Cu zx in the other, and, in particular, to hopping via yttrium.

The bands resulting from diagonalization of the 8-band Hamiltonian with the odd and even set of parameters are shown in Figs. 6(c) and 6(d), respectively. The agreement between these model bands and the original LDA bands in Figs. 4(c) and 4(d) is reasonably good over the 4 eV range shown, which indicates that our model is physically sound. Close to the Fermi level, where the bands were actually fitted, the agreement is of course much better. This is illustrated in Fig. 7 which compares the plane-band Fermi surface and the constant energy surfaces ±30 meV away for the *ab initio* bands [Figs. 4(c) and 4(d)] in the left-hand side with those of the 8-band model in the right-hand side. There is hardly a difference. The difference is somewhat larger to the appropriate cross sections $(o,0)$ and $(e,\pi/c)$ in the left-hand side of Fig. 2 calculated with a complete basis set and the full potential, but this is mainly due to our deliberate neglect of chain $pd\pi$ orbitals in the model. In Sec. V A, we shall give an analytical expression for the constant energy surfaces shown in the right-hand side of Fig. 7.

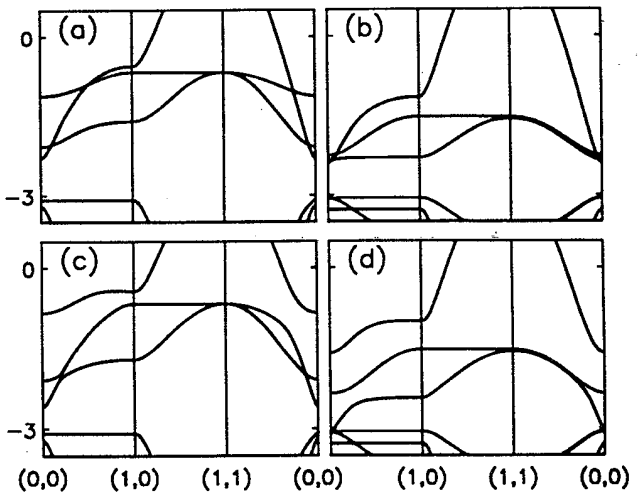

FIG. 6. Results of the 8-band model for the odd [left panel (a) and (c)] and even [right panel (b) and (d)] plane bands. In (a) and (b) the couplings t_a and t_b between the hybridized $pd\sigma$-$sp\sigma$ bands and the $pd\pi$ bands was set to zero, but not in (c) and (d). Figures (c) and (d) model respectively Figs. 4(c) and 4(d).

In Figs. 6(a) and 6(b) we have set $t_a = t_b = 0$ and thus neglected the coupling between the $pd\sigma$ and $pd\pi$ bands. In this sense, these two figures are appropriate for flat, undimpled planes. The $pd\sigma$ bands are now seen to have normal k^2 saddle points at (1,0). Compared with Figs. 6(c) and 6(d), this exhibits the bifurcation mechanism. Figure 6(a) is the model for the superposition of Figs. 4(e) and 4(g), and Fig. 6(b) is the model for the superposition of Figs. 4(f) and 4(h). We see that the present model does not describe the even $pd\pi$ bands [Fig. 4(h)] well; our fitting merely achieves to get the upper band right between (0,0) and (1,0) which is what matters for the $pd\sigma$ band, once $t_a \neq 0$.

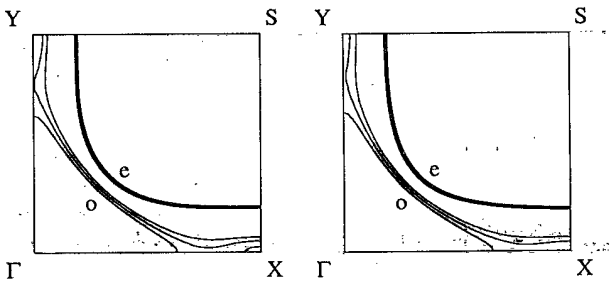

FIG. 7. FS and constant energy surfaces corresponding to $\epsilon = \epsilon_F \pm 30$ meV for $YBa_2Cu_3O_7$, calculated with the LMTO-ASA method and the 2×7 basis (left), and with the 8-band model equation (12) (right). The corresponding energy bands are those shown in respectively Figs. 4(c) and 4(d), and in Figs. 6(c) and 6(d).

For certain applications, e.g., in calculations which include the on-site Cu Coulomb energy U, it is most convenient to keep only the dominant Cu orbital, x^2-y^2, and hence to downfold the Cu s, zx, and zy orbitals. The resulting *5-band Hamiltonian* then equals H^8, except that the s, zx, and zy rows and columns are canceled and that

$$\langle x|H^5|x\rangle = \epsilon_x - \frac{t_{sx}^2}{\epsilon_s - \epsilon} s_x^2,$$

$$\langle x|H^5|y\rangle = -\frac{t_{sx}t_{sy}}{\epsilon_s - \epsilon} s_x s_y,$$

$$\langle y|H^5|y\rangle = \epsilon_y - \frac{t_{sy}^2}{\epsilon_s - \epsilon} s_y^2,$$

$$\langle za|H^5|za\rangle = \epsilon_{za} + \frac{t_{z,zx}^2}{\epsilon - \epsilon_{zx}} s_x^2,$$

$$\langle zb|H^5|zb\rangle = \epsilon_{zb} + \frac{t_{z,zy}^2}{\epsilon - \epsilon_{zy}} s_y^2,$$

with ϵ approximated by a constant, e.g., the Fermi energy. This approximation is a good one. H^5 thus includes O-O nearest- and second-nearest-neighbor hoppings via copper (plus shifts of the on-site oxygen energies).

IV. FOUR-BAND ($pd\sigma, pd\pi, sp\sigma$) HAMILTONIAN

Next, we derive simple analytical expressions for the $pd\sigma$, $pd\pi$, and $sp\sigma$ bands and for the constant energy contours (CEC's) in (k_x, k_y) space, especially those of the Fermi surface (Fig. 7). This provides a detailed understanding of the bands, the Fermi surface, and of the nature of the saddle points. We start from H^8 and downfold the x, y, zx, and zy orbitals exactly. This produces a "physical" 4-band Hamiltonian $H^4(\epsilon)$ whose most relevant element is the diagonal one for the $pd\sigma$ orbital:

$$\begin{aligned}\langle d|H^4|d\rangle &= \epsilon_d + \frac{t_{xd}^2 s_x^2}{\epsilon - \epsilon_x} + \frac{t_{yd}^2 s_y^2}{\epsilon - \epsilon_y} \\ &\equiv \epsilon + (\epsilon - \epsilon_d)\left[-1 + xD_a(\epsilon) + yD_b(\epsilon)\right].\end{aligned}$$

Here, and in the following, we use

$$(x, y) \equiv \left\{\sin^2(k_x a/2), \sin^2(k_y b/2)\right\} = \left(s_x^2, s_y^2\right)/4 \quad (5)$$

as the variable for the two-dimensional *Bloch vector*. In (x, y) space, the irreducible zone is mapped onto the (0|1) square. In the expression for $\langle d|H^4|d\rangle$ the $pd\sigma$-like interactions are described by the following *functions of energy:*

$$\begin{aligned}D_a(\epsilon) &\equiv \frac{4t_{xd}^2}{(\epsilon - \epsilon_x)(\epsilon - \epsilon_d)}, \\ D_b(\epsilon) &\equiv \frac{4t_{yd}^2}{(\epsilon - \epsilon_y)(\epsilon - \epsilon_d)}.\end{aligned} \quad (6)$$

These functions are positive and decreasing in the energy range of interest. The equation $\epsilon = \langle d|H^4|d\rangle$ yields the usual 3-band model without O-O hopping: Neglecting orthorhombicity and setting $\epsilon_d = \epsilon_x = \epsilon_y \equiv \epsilon_p$, we get $\epsilon = \epsilon_p + 2t_{pd}\sqrt{x+y}$ for the antibonding $pd\sigma$ band, which is the usual expression. The bottom of this band is at (0,0), the saddle points are at (1,0) and (0,1), and the top is at (1,1). When the energy increases from the bottom, via the saddle point, to the top of the band, $D(\epsilon)$ thus decreases from ∞, via 1, to 1/2. With our parameter values for $YBa_2Cu_3O_7$, we have $D_a^o(\epsilon_F)$=1.89 and $D_b^o(\epsilon_F)$= 1.92 for the odd band, and $D_a^e(\epsilon_F)$=1.68 and $D_b^e(\epsilon_F)$= 1.78 for the even band.

We may express the diagonal element for the $sp\sigma$ orbital in a similar way, i.e.,

$$\langle s|H^4|s\rangle - \epsilon = (\epsilon_s - \epsilon)\left[1 + xS_a(\epsilon) + yS_b(\epsilon)\right]$$

where the $sp\sigma$ interactions are described by the function

$$S_a(\epsilon) \equiv \frac{4t_{sx}^2}{(\epsilon_s - \epsilon)(\epsilon - \epsilon_x)} \quad (7)$$

and similarly for $S_b(\epsilon)$. Note, that we have chosen the sign such that S is positive in the range of interest. At the Fermi energy in $YBa_2Cu_3O_7$, $S_a^o(\epsilon_F)$=1.12 and $S_b^o(\epsilon_F)$=1.15 for the odd band, and $S_a^e(\epsilon_F)$=2.30 and $S_b^e(\epsilon_F)$=2.34 for the even band. This large difference is due to the interplane hopping integral between the Cu s orbitals. Since $t_{sp} > t_{pd}$, S can be larger than D. The matrix element between the $pd\sigma$ and $sp\sigma$ orbitals is

$$\left\langle s\middle|H^4\middle|d\right\rangle = \sqrt{\left(\epsilon_s - \epsilon\right)\left(\epsilon - \epsilon_d\right)}\left[x\sqrt{S_a\left(\epsilon\right)D_a\left(\epsilon\right)} - y\sqrt{S_b\left(\epsilon\right)D_b\left(\epsilon\right)}\right],$$

and this causes the $pd\sigma$ band to be *depressed* by the above-lying $sp\sigma$ band, except near the x=y diagonal. The depression is strongest at the (1,0) and (0,1) saddle points where, for the pure $pd\sigma$ band we had $D = 1$, and now $D = 1 + S$. This latter equation is in fact Eq. (3) used for the initial parameter fit. The $sp\sigma$-hybridized $pd\sigma$ band is the model for Figs. 4(e) and 4(f), and is shown for our parameter values as three of the bands in Figs. 6(a) and 6(b).

Due to the above-mentioned depression, the $pd\sigma$ band approaches the top of the one-dimensional $pd\pi$ bands stretching along the $(1,y)$ and $(x,1)$ lines as seen in Figs. 6(a) and 6(b). The $pd\pi$ bands are described by

$$\langle za|H^4|za\rangle - \epsilon = (\epsilon - \epsilon_{za})\left[-1 + xZ_a(\epsilon)\right]$$

and similarly for $\langle zb|H^4|zb\rangle$ with

$$Z_a(\epsilon) \equiv \frac{4t_{z,xz}^2}{(\epsilon-\epsilon_{xa})(\epsilon-\epsilon_{xz})}, \tag{8}$$

and similarly for $Z_b(\epsilon)$. For the odd bands and at the Fermi level in $YBa_2Cu_3O_7$, $Z_a^o(\epsilon_F)=Z_b^o(\epsilon_F)=0.72$, while for the even bands $Z_a^e(\epsilon_F)=0.24$ and $Z_b^e(\epsilon_F)=0.22$. This large difference reflects the strong interplane O z - O z hopping and the asymmetric coupling through yttrium. The $pp\pi$ coupling seen in Figs. 4(i) and 4(j), in particular for the odd band, is described by the matrix element

$$\begin{aligned}\langle za|H^4|zb\rangle &= -4t_{zz}\sqrt{(1-x)(1-y)} \\ &\equiv -\sqrt{(\epsilon-\epsilon_{za})(\epsilon-\epsilon_{zb})} \\ &\times \sqrt{(1-x)(1-y)P(\epsilon)}\end{aligned}$$

and the function

$$P(\epsilon) \equiv \frac{16t_{zz}^2}{(\epsilon-\epsilon_{za})(\epsilon-\epsilon_{zb})}. \tag{9}$$

For $YBa_2Cu_3O_7$, $P^o(\epsilon_F)=0.16$ for the odd band, and negligible for the even band.

The matrix element which causes saddle-point bifurcation when the $sp\sigma$ depression makes the $pd\sigma$ and $pd\pi$ bands nearly degenerate is

$$\langle za|H^4|d\rangle = \sqrt{(\epsilon-\epsilon_{za})(\epsilon-\epsilon_d)}\sqrt{(1-x)T_a(\epsilon)},$$

and analogously for $\langle zb|H^4|d\rangle$, although with a change of sign. The weak interactions between the x^2-y^2 and the z orbitals are here described by

$$T_a(\epsilon) \equiv \frac{4t_a^2}{(\epsilon-\epsilon_{za})(\epsilon-\epsilon_d)} \tag{10}$$

and $T_b(\epsilon)$. At the Fermi level in $YBa_2Cu_3O_7$, $T_a^o(\epsilon_F)=0.093$ and $T_b^o(\epsilon_F)=0.089$ for the odd bands, and $T_a^e(\epsilon_F)=0.076$ and $T_b^e(\epsilon_F)=0.066$ for the even bands. This difference again reflects the largeness of the interplane O z - O z hopping integral.

The 4-band $pd\sigma$, $sd\sigma$, $pd\pi$ Hamiltonian may therefore be obtained from

$$\frac{H_{ij}^4(\epsilon)-\epsilon\delta_{ij}}{\sqrt{(\epsilon-\epsilon_i)(\epsilon-\epsilon_j)}} =$$

$$\begin{pmatrix} -1+xD_a+yD_b & x\sqrt{D_aS_a}-y\sqrt{D_bS_b} & \sqrt{(1-x)T_a} & -\sqrt{(1-y)T_b} \\ x\sqrt{D_aS_a}-y\sqrt{D_bS_b} & 1+xS_a+yS_b & 0 & 0 \\ \sqrt{(1-x)T_a} & 0 & -1+xZ_a & -\sqrt{(1-x)(1-y)P} \\ -\sqrt{(1-y)T_b} & 0 & -\sqrt{(1-x)(1-y)P} & -1+yZ_b \end{pmatrix} \tag{11}$$

where we have dropped the energy argument of the potential functions D, S, Z, P, and T. This energy dependent Hamiltonian is exactly equivalent with the 8-band Hamiltonian (2).

V. ONE-BAND HAMILTONIAN

A. Constant energy contours

The equation for the CEC's may now be obtained by downfolding $\left[H_{ij}^4(\epsilon)-\epsilon\delta_{ij}\right]/\sqrt{(\epsilon-\epsilon_i)(\epsilon-\epsilon_j)}$ to an effective, energy-dependent *one-band Hamiltonian.* The result is:

$$\begin{aligned}0 = \frac{\langle d|H^1|d\rangle-\epsilon}{\epsilon-\epsilon_d} &= -1+xD_a+yD_b-\frac{\left(x\sqrt{D_aS_a}-y\sqrt{D_bS_b}\right)^2}{1+xS_a+yS_b} \\ &+\frac{(1-yZ_b)(1-x)T_a+(1-xZ_a)(1-y)T_b+(1-x)(1-y)2\sqrt{PT_aT_b}}{(1-yZ_b)(1-xZ_a)-(1-x)(1-y)P}\end{aligned} \tag{12}$$

where, again, we have dropped the energy argument of the potential functions D, S, Z, P, and T, and the energy-dependent one-band Hamiltonian is exactly equivalent with the 8-band Hamiltonian (2).

The expression simplifies if we can neglect the $pp\pi$ hopping (P=0) which couples the (z,zx) and (z,zy) $pd\pi$ bands. In this case, the last term reduces to

$$\frac{(1-x)T_a}{1-xZ_a}+\frac{(1-y)T_b}{1-yZ_b}. \tag{13}$$

If, in addition, we are willing to neglect the $pd\pi$-dispersion (Z=0), this term is just

$$(1-x)T_a+(1-y)T_b. \tag{14}$$

The x and y coordinates were defined in (5) and the physical irreducible zone corresponds to the square: (x,y)=(0,0), (1,0), (0,1), (1,1). *It is thus the* $\sin^2$ *mapping* (5) *which produces the space-group symmetry of* $\epsilon(\mathbf{k})$. The CEC equation (12) clearly exhibits the effects of the

various physical parameters on the band structure, as may be realized from the following tutorial:

In the usual, tetragonal 3-band $pd\sigma$ model without O-O hopping, only D_a=D_b is nonzero so that the CEC equation reduces to

$$1 = (x + y)\, D. \tag{15}$$

This is a set of straight lines in (x,y) space. In **k**-space, it gives $ak_x + bk_y = \pi$ when $D = 1$, and this is the well-known [11]-oriented, square Fermi contour for half filling (in the absence of a Coulomb gap) with corners (crossings in the repeated zone) at the $(\pi/a, 0)$ and $(0, \pi/b)$ saddle points. It is shown by the dashed lines in Fig. 1. For D increasing beyond 1, the CEC's are electron pockets shrinking around $(0, 0)$ and, for D decreasing from 1 to 1/2, the CEC's are hole pockets shrinking around $(\pi/a, \pi/b)$.

If we now include the hybridization with the $sp\sigma$ orbital (i.e., $S > 0$), the bands become like those shown in Figs. 4(e) and 4(f) and in Figs. 6(a) and 6(b). The CEC's are given by:

$$1 = (x + y)\,(D - S) + 4xyDS, \tag{16}$$

which are *hyperbola's* in (x,y) space with [10]- and [01]-oriented asymptotes. As long as the number of holes is not too large, the CEC's in **k** space tend to be $(\pi/a, \pi/b)$-centered hole pockets, shaped like rounded squares, *but now with* [10]-[01] *orientation.* This is the "normal" shape of those real $YBa_2Cu_3O_7$ constant energy contours whose energy is well above the saddle points, i.e., the CEC's (e) and $(o,\pi/c)$ in Fig. 2. For the $pd\sigma - sd\sigma$ model that we are considering, the saddle points remain at $(\pi/a, 0)$ and $(0, \pi/b)$ because, with orthogonal asymptotes, the hyperbola cannot *touch* the x or y axis. The interaction with the above-lying $sp\sigma$ band has pushed the saddle-point energies down corresponding to $1 = D - S$. When the hole count is increased such that the energy falls below the saddle points, the CEC's become the Γ-centered electron jacks. Both shapes are well-known Fermi-energy contours in tetragonal La_2CuO_4.

Next, we consider the pure $pd\pi$ bands, like the ones shown in Fig. 6(b) for which $t_{zz} \approx 0$ and $t_a \equiv t_b \equiv 0$. We therefore set all parameters, except $Z_a = Z_b$, equal to zero. The corresponding CEC's,

$$1 = xZ \quad \text{and} \quad 1 = yZ,$$

are two sets of straight lines running parallel with the axes. From the bottom to the top of the $pd\pi$-bands, Z therefore decreases from ∞ to 1. If now the top of the (z,zx) band, which extends along the $(1,y)$ line, comes close to the above-lying $pd\sigma$ band, and this can only occur near the (1,0) saddle point of the latter, then weak $pd\sigma - pd\pi$ interaction introduced through a dimple of O2 can push the conduction band up by a significant amount, except along $(1,y)$ where the orbitals cannot mix. This is the case described by expression (13). If sufficiently strong, this mechanism will cause the saddle point to move from (1,0) to $(\bar{x},0)$. This just about occurs when going from Figs. 6(b) to 6(d). In **k** space, the mirror plane through $(\pi/a,0)$ and perpendicular to [10] makes the saddle point first *extend* and then *bifurcate.* A prerequisite for this mechanism is thus that the energy of the $pd\sigma$ band has been depressed in energy near the saddle point by the Cu s interaction, otherwise its energy would have been far above the top of the (z,zx) band. In terms of the interaction parameters, this near-degeneracy condition is $\bar{D} - \bar{S} \approx \bar{Z}$, where the overbar refers to the saddle-point energy.

If we couple the two $pd\pi$ orbitals through hopping between the O2 z and O3 z orbitals ($P \neq 0$), a gap opens at (0,0) and the dispersion along $(x, 0)$ changes considerably, as seen by comparison of Figs. 6(b) and 6(a). The saddle-point bifurcation thus depends on such details. One might believe that the most simple description of the situation seen in Fig. 6(a) for the odd bands is to let the O z bands be flat, that is, to use $P = 0$ *and* $Z = 0$, i.e., expression (14). This, however, makes the O2 and O3 z orbitals degenerate and will therefore have the effect of repelling the $pd\sigma$ band, not only away from, but also *at* (1,0) and (0,1). The tendency to bifurcation will thus be diminished.

In general, Eq. (12) for the CEC's is a *polynomial*

$$\mathsf{A}x + \mathsf{B}y + \mathsf{C}xy - \mathsf{D}x^2 - \mathsf{E}y^2$$

$$-\mathsf{F}x^2y - \mathsf{G}xy^2 + \mathsf{H}x^2y^2 = \mathsf{I} \tag{17}$$

of up to *second power* in x and in y; the higher powers drop out. Any CEC is therefore described by 8 normalized coefficients. The fastest way of computing the CEC's is presumably to find their intersection with lines parallel with x (or y) axis by writing the polynomial equation (17) as

$$\left(-\mathsf{D} - \mathsf{F}y + \mathsf{H}y^2\right) x^2 + \left(\mathsf{A} + \mathsf{C}y - \mathsf{G}y^2\right) x$$

$$+ \left(-\mathsf{I} + \mathsf{B}y - \mathsf{E}y^2\right) = 0.$$

In order to obtain the explicit expressions for the coefficients in terms of the potential functions, we need to perform the multiplications with the denominators in the expression for $\langle d \left| H^1 \right| d \rangle$. The result is

$$
\begin{aligned}
\mathsf{A} &= (D_a - S_a)(1-P) + (Z_a - P) + S_a\left(T_a + T_b + 2\sqrt{PT_aT_b}\right) - \left(T_a + Z_aT_b + 2\sqrt{PT_aT_b}\right), \\
\mathsf{C} &= -(D_a - S_a)(Z_b - P) - (D_b - S_b)(Z_a - P) + 4DS(1-P) - (Z_aZ_b - P) \\
&\quad -S_a\left(T_b + Z_bT_a + 2\sqrt{PT_aT_b}\right) - S_b\left(T_a + Z_aT_b + 2\sqrt{PT_aT_b}\right) + \left(Z_aT_b + Z_bT_a + 2\sqrt{PT_aT_b}\right) \\
\mathsf{D} &= (D_a - S_a)(Z_a - P) + S_a\left(T_a + Z_aT_b + 2\sqrt{PT_aT_b}\right), \qquad (18) \\
\mathsf{F} &= -(D_a - S_a)(Z_aZ_b - P) + 4DS(Z_a - P) - S_a\left(Z_aT_b + Z_bT_a + 2\sqrt{PT_aT_b}\right), \\
\mathsf{H} &= 4DS(Z_aZ_b - P), \\
\mathsf{I} &= 1 - P - \left(T_a + T_b + 2\sqrt{PT_aT_b}\right).
\end{aligned}
$$

The expressions for B, E, and G may be obtained from those for, respectively, A, D, and F by interchange of the subscripts a and b. Furthermore, we have made use of the definition:

$$4DS \equiv D_aS_b + D_bS_a + 2\sqrt{D_aD_bS_aS_b}.$$

The values of these parameters *at the Fermi level* are:

	A	B	C	D	E	F	G	H	I
o	1.255	1.270	5.689	0.686	0.697	4.303	4.326	3.088	0.581
e	−0.136	−0.084	15.908	0.075	0.080	3.751	3.484	0.831	0.853

for respectively the odd and even plane bands.

B. Condition for extended saddle points

The strict condition for *bifurcation* of the *saddle point* along the $(x,0)$ line is that the CEC *touches* the line at a value $\bar{x} \leq 1$. The saddle point is *extended* when $\bar{x} = 1$.

Now, the intersections with the $(x,0)$ line are given by

$$x = \left(\mathsf{A} \pm \sqrt{\mathsf{A}^2 - 4\mathsf{DI}}\right)/2\mathsf{D},$$

and the necessary and sufficient condition for saddle-point *bifurcation* along $(k_x,0)$ is therefore that there exists an energy $\bar{\epsilon}$, for which the values $\bar{\mathsf{I}}$, $\bar{\mathsf{A}}$, and $\bar{\mathsf{D}}$ of the functions $\mathsf{I}(\epsilon)$, $\mathsf{A}(\epsilon)$, and $\mathsf{D}(\epsilon)$ satisfy

$$\bar{x} = \frac{\bar{\mathsf{A}}}{2\bar{\mathsf{D}}} = \frac{2\bar{\mathsf{I}}}{\bar{\mathsf{A}}} = \sqrt{\frac{\bar{\mathsf{I}}}{\bar{\mathsf{D}}}} \leq 1.$$

The necessary and sufficient condition that the saddle point is *extended*, is that $\bar{\mathsf{A}}/2 = \bar{\mathsf{D}} = \bar{\mathsf{I}}$, for the energy $\bar{\epsilon} = \epsilon(1,0)$ of the X point. Of these two equations, $\bar{\mathsf{D}} + \bar{\mathsf{I}} = \bar{\mathsf{A}}$ yields the energy of the X point and, in terms of the basic interaction functions (6), (7), and (10), this equation becomes:

$$\bar{D}_a = \left(1 + \bar{S}_a\right)\left(1 - \bar{T}_b\right), \qquad (19)$$

as seen by use of Eq. (19), or directly from Eq. (12). This simple equation (19) is the generalization of Eq. (3) to the full 8-band model, and it shows that the energy of the planelike band at the X point is independent of Z and P, for instance. In order to get a feeling for the numbers, we may compare the values for the odd interaction functions at the Fermi energy calculated in Sec. IV with Eq. (19), noting that the Fermi energy is less than 30 meV above the energy of the odd plane band at the X point (see the right part of Fig. 7). The result is that the value of $D_a(\epsilon_F) = 1.89$ is, indeed, just slightly smaller than the value of $[1 + S_a(\epsilon_F)][1 - T_b(\epsilon_F)] = 2.12 \times 0.911 = 1.93$.

We now insert Eq. (19) in the other equation $(\bar{\mathsf{D}} = \bar{\mathsf{I}})$ and thus obtain an expression for the value of the O z - Cu $x^2 - y^2$ hopping integral t_a which is necessary and sufficient for the saddle point at X to be *extended*. This expression, in terms of the interaction functions defined in (10), (9), (8), and (6), is

$$\sqrt{\bar{T}_a} = \left(1 - \bar{T}_b\right)\sqrt{\left(1 - \bar{Z}_a\right)/\bar{D}_a} - \sqrt{\bar{P}\bar{T}_b}. \qquad (20)$$

If the value of $\sqrt{\bar{T}_a}$ is smaller than that of the right-hand side, the saddle point at X will be normal, and if the value of $\sqrt{\bar{T}_a}$ is larger than that of the right-hand side, the saddle point will bifurcate away from X. Here again, we may insert the values of the odd interaction function at the Fermi energy. We find that the value of $\sqrt{T_a(\epsilon_F)} = 0.305$ is larger than that of $[1 - T_b(\epsilon_F)]\sqrt{[1 - Z_a(\epsilon_F)]/D_a(\epsilon_F)} - \sqrt{P(\epsilon_F)T_b(\epsilon_F)} = 0.911\sqrt{0.280/1.89} - \sqrt{0.16 \cdot 0.089} = 0.351 - 0.119 = 0.232$. This is consistent with the fact that this saddle point is bifurcated.

The expressions for the saddle point along the $(0,y)$ line are analogous to those given above with exchange of the subscripts a and b. For our values of the parameters, we see from Fig. 7 that the saddle point of the odd plane band along $(0,y)$ is extended and has an energy very close to ϵ_F, and slightly above that of the Y point. As regards the energy at the

Y point, we have $D_b(\epsilon_F) = 1.92$, which is, indeed, just slightly smaller than $[1+S_b(\epsilon_F)][1-T_a(\epsilon_F)] = 2.15 \times 0.907 = 1.95$. As regards the nature of the saddle point, we have: $\sqrt{T_b(\epsilon_F)} = 0.298$, which is larger than $[1-T_a(\epsilon_F)]\sqrt{[1-Z_b(\epsilon_F)]/D_b(\epsilon_F)} - \sqrt{P(\epsilon_F)T_a(\epsilon_F)} = 0.907\sqrt{0.280/1.92} - \sqrt{0.16 \cdot 0.093} = 0.346 - 0.122 = 0.224$, and thus consistent with the fact that the saddle point is bifurcated.

VI. A SIMPLE MATHEMATICAL MODEL FOR THE CEC'S

The model for the CEC's presented in the previous section and expressed by (17) is, in our opinion, the simplest possible model containing the correct single-particle physics. For many purposes this model may, however, seem too complicated and we can therefore not avoid mentioning that the *circle*

$$[x-(1-\Delta)]^2 + [y-(1-\Delta)]^2 = (1-\Delta)^2(1-\epsilon/w)^2$$

in (x,y) space gives normal saddle points at (1,0) and (0,1) for $\Delta < 0$, extended saddle points for $\Delta = 0$, and bifurcated saddle points for $\Delta > 0$. This circle is centered at $(1-\Delta, 1-\Delta)$ and has the radius $(1-\Delta)(1-\epsilon/w)$ so that it touches the axes at (1−Δ,0) and (0,1−Δ) for $\epsilon = 0$. The maximum is at $(x,y) = (1-\Delta, 1-\Delta)$ and has energy w. When the touching points are inside the physical square, $0 \le x \le 1$, $0 \le y \le 1$, the saddle points in (k_x, k_y) space [see Eq. (5)] become extended or bifurcated. Three constant energy contours of this model with parameter values Δ=0.15 and $\epsilon = 0$ and $\pm 0.05w$ are shown in Fig. 8. The similarity with the physical model and with the full LDA calculations is striking.

The advantages of this circle in (x,y) space over the k-space circle in Fig. 1 is that only the former describes the CEC's for energies away from the saddle points and describes normal, extended, and bifurcated saddle points with one model.

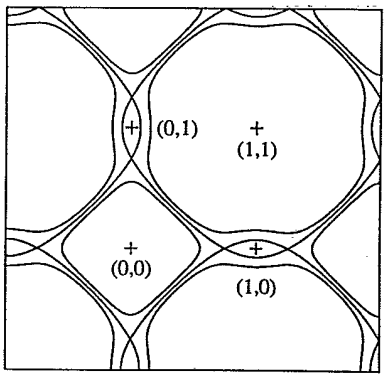

FIG. 8. FS and constant energy surfaces in (k_x, k_y) space of the mathematical model presented in Sec. VI. The parameters were Δ=0.15 and ϵ=0 and $\pm 0.05w$.

VII. SPIN FLUCTUATIONS

At the end, we return to Fig. 5 and comment on the observation, mentioned in the Introduction, that in optimally doped $YBa_2Cu_3O_7$, the spin fluctuations are antiferromagnetic and commensurable inside each plane *and* antiferromagnetic *between* the planes.[18] For a FS with energy 20 meV below an extended saddle point at (1,0) and 20 meV above an extended saddle point at (0,1), we expect the orbitals of a spin fluctuation inside a single plane to be $\psi(1,0)\pm\psi(0,1)$ as shown in the two bottom right-hand panels; one orbital is for the spin-up and the other for the spin-down electron. Note that the intra-plane antiferromagnetism has separated the Cu *s* and Cu *d* characters onto different sublattices. One consequence is that the screening of the Coulomb correlations among the *d* electrons by the *s* electrons is intraatomic in the metallic state (top figure) but interatomic, and hence weaker, in the antiferromagnetic state. Consider now a double plane. The spin-up orbitals of spin fluctuations coupled ferromagnetically (F) and antiferromagnetically (A) across the planes (denoted + and −) are given by: $2\Psi_{F/A} = [\psi(1,0)+\psi(0,1)]_- - [\psi(1,0)\pm\psi(0,1)]_+$. From the figure, one would, in the first place, expect the F coupling to be strongest because it lines the Cu *s* sublattices up on top of each other and thus allows vertical Cu *s* hopping between the planes. However, this neglects the important (O2 *z*, Cu *zx*)(1,0) and (O3 *z*, Cu *zy*)(0,1) degrees of freedom whose bands in the metallic state were close in energy to the odd $pd\sigma$ band and which were responsible for the bifurcation of the saddle points, away from (1,0) and (0,1) (see Figs. 4 and 6). These $pd\pi$ components are symmetry forbidden in $\psi(1,0)$ and $\psi(0,1)$, but *not* in $\psi(1,0)\pm\psi(0,1)$ and their coupling across the double plane is much stronger than their coupling to the $pd\sigma$ band, as we have seen. Moreover, we found the Cu *zx* - Cu *zx* and Cu *zy* - Cu *zy* couplings to be *negative,* presumably due to hopping through yttrium, and therefore to favor antiferromagnetic interplane coupling. We thus expect the plane-oxygen *z* degrees of freedom to be important not only for the ground-state saddle points, but also for the interplane coupling of the spin fluctuations.

VIII. CONCLUSION

In conclusion, we have identified *plane oxygen z* as the electronic degrees of freedom responsible for the predicted and observed anomalous flatness of the saddle points and their pinning to ϵ_F in optimally doped materials. These electronic degrees of freedom are activated by plane dimpling and they couple across double planes. For use in future studies, we have derived appropriate tight-binding Hamiltonians, as well as analytical expressions for the constant-energy contours near the Fermi surface.

ACKNOWLEDGEMENT

We have enjoyed fruitful discussions with J.C. Campuzano.

[1] Rong Liu, B.W. Veal, A.P. Paulika, J.W. Downey, H. Shi, C.G. Olson, C. Gu, A.J. Arko, and J.J. Joyce, Phys. Rev. B **45**, 5614 (1992).
[2] R. Manzske, G. Mante, R. Claessen, M. Skibowski, and J. Fink, Surf. Sci. **269-272**, 1066 (1992).
[3] Z.-X Shen, D.S. Dessau, B.O. Wells, D.M. King, W.E. Spicer, A.J. Arko, D. Marshall, L.W. Lomberdo, A. Kapitulnik, P. Dickinson, S. Doniach, J. DiCarlo, A.G. Loeser, and C.H. Park, Phys. Rev. Lett. **70**, 1553 (1993).
[4] K. Gofron, J.C. Campuzano, H. Ding, R. Liu, A.A. Abrikosov, D.D. Koelling, B. Dabrowski, and B.W. Veal (unpublished).
[5] W.E. Pickett, R.E. Cohen, and H. Krakauer, Phys. Rev. B **42**, 8764 (1990).
[6] O.K. Andersen, A.I. Liechtenstein, C.O. Rodriguez, I.I. Mazin, O. Jepsen, V.P. Antropov, O. Gunnarsson, and S. Gopalan, Physica C **185-189**, 147 (1991).
[7] Rong Liu, B.W. Veal, A.P. Paulika, J.W. Downey, P.J. Kostic, S. Flesher, U. Welp, C.G. Olson, X. Wu, A.J. Arko, and J.J. Joyce, Phys. Rev. B **46**, 11056 (1992).
[8] L.C. Smedskjaer, A. Bansil, U. Welp, Y. Fang, and K.G. Bailey, Phys. Rev. B **46**, 5868 (1992); H. Haghighi, J.H. Kaiser, S. Rayner, R.N. West, J.z. Liu, R. Shelton, R.H. Howell, F. Solal, and M.J. Fluss, Phys. Rev. Lett. **67**, 382 (1991).
[9] C.M. Fowler, B.L. Freeman, W.L. Hults, J.C. King, F.M. Mueller, and J.L. Smith, Phys. Rev. Lett. **68**, 534 (1992); F.M. Mueller, C.M. Fowler, B.L. Freeman, W.L. Hults, J.C. King, and J.L. Smith, *ibid.* **68**, 3937 (1992); F.M. Mueller, A.J. Arko, P.C. Canfield, K.T. Christensen, W. Ferenbaugh, C.M. Fowler, B.L. Freeman, W.L. Hults, J.C. King, J.L. Smith, S. Askenazy, R.G. Goodrich, D. Hall, D.H. Lowndes, E. Haanappel, J.H. Kim, I. Vagner, and P. Wyder, Phys. Rev. Lett. **69**, 2454 (1992).
[10] I.I. Mazin, O. Jepsen, O.K. Andersen, and A.I. Liechtenstein, Phys. Rev. Lett. **68**, 3936 (1992); I.I. Mazin, O. Jepsen, O.K. Andersen, A.I. Liechtenstein, S.N. Rashkeev, and Y.A. Uspenskii, Phys. Rev. B **45**, 5103 (1992).
[11] C.O. Rodriguez, A.I. Liechtenstein, O. Jepsen, I.I. Mazin, and O.K. Andersen, Comp. Mater. Sci. (to be published).
[12] D.M. Newns, C.C. Tsuei, P.C. Pattnaik, C.L. Kane, Comments Condens. Matter Phys. **XV** 273 (1992); C.C. Tsuei, C.C. Chi, D.M. Newns, P.C. Pattnaik, and M. Däumling, Phys. Rev. Lett. **69**, 2134 (1992).
[13] R.S. Markiewicz, Int. J. Mod. Phys. B **5**, 2037 (1991).
[14] S. Gopalan, O. Gunnarsson, and O.K. Andersen, Phys. Rev. B **46**, 11798 (1992).
[15] D.M. Newns, H.R. Krishnamurthy, P.C. Pattnaik, C.C. Tsuei, and C.L. Kane, Phys. Rev. Lett. **69**, 1264 (1992).
[16] A.A. Abrikosov, J.C. Campuzano, and K. Gofron, Physica C **214**, 73 (1993).
[17] H.A. Mook, M. Yethiraj, G. Aeppli, T.E. Mason, and T. Armstrong, Phys. Rev. Lett. **70**, 3490 (1993).
[18] J. Rossat-Mignod, L.P. Regnault, C. Vettier, P. Bourges, P. Burlet, J. Bossy, J.Y. Henry, and G. Lapertot, Physica B **180-181**, 383 (1992); J. Rossat-Mignod, L.P. Regnault, P. Bouges, P. Burlet, C. Vettier, and J.Y. Henry, Phys. Rev. Lett. **70**, 3490 (1993).
[19] C.O. Rodriguez, A.I. Liechtenstein, I.I. Mazin, O. Jepsen, and O.K. Andersen, J. Phys.: Condens. Matter **5**, A377 (1993).
[20] U. Welp, M. Grimsditch, S. Fleshler, W. Nessler, J. Downey, G.W. Crabtree, and J. Guimpel, Phys. Rev. Lett. **69**, 2130 (1992).
[21] C.O. Rodriguez, A.I. Liechtenstein, I.I. Mazin, O. Jepsen, O.K. Andersen, and M. Methfessel, Phys. Rev. B **42**, 2692 (1990).
[22] I.I. Mazin, O.K. Andersen, A.I. Liechtenstein, O. Jepsen, V.P. Antropov, S.N. Rashkeev, V.I. Anisimov, J. Zaanen, C.O. Rodriguez, and M. Methfessel, in *Lattice Effects in High-T_c Superconductors*, edited by Y. Bar-Yam, T. Egami, J. Mustre-de Leon, and A.R. Bishop (World Scientific, Singapore, 1992), p. 235.
[23] A.I. Liechtenstein, I.I. Mazin, O. Jepsen, F. Poulsen, and O.K. Andersen (unpublished).
[24] C. Thomsen, and M. Cardona, in *High-Temperature Superconductors I and II*, edited by D.M. Ginsberg (World Scientific, Singapore, 1990).
[25] S.L. Cooper, M.V. Klein, B.G. Pazol, J.P. Rice, and D.M. Ginsberg, Phys. Rev. B **37**, 5920 (1988).
[26] C. Thomsen, M. Cardona, B. Friedl, C.O. Rodriguez, I.I. Mazin, and O.K. Andersen, Solid State Commun. **75**, 219 (1990); B. Friedel, C. Thomsen, H.-U. Habermeier, and M. Cardona, Solid State Commun. **81**, 989 (1992).
[27] L. Pietronero and S. Strässler, Europhys. Lett. **18**, 627 (1992).
[28] O.K. Andersen and O. Jepsen, Phys. Rev. Lett. **53**, 2571 (1984); W.R.L. Lambrecht and O.K. Andersen, Phys. Rev. B **34**, 2439 (1986); the present calculations included the combined correction in the downfolding procedure as explained in O.K. Andersen, A.V. Postnikov, and S.Yu. Savrasov, in *Applications of Multiple Scattering Theory to Materials Science*, edited by W. H. Butler, P. H. Dederichs, and A. Gonis, and R. L. Weaver, MRS Symposia Proceedings No. 253 (Materials Research Society, Pittsburgh, 1992), p. 37; and more clearly in O.K. Andersen, T. Paxton, and O. Jepsen (unpublished).